

## Chapter 5

### Resonant superfluid Fermi gases

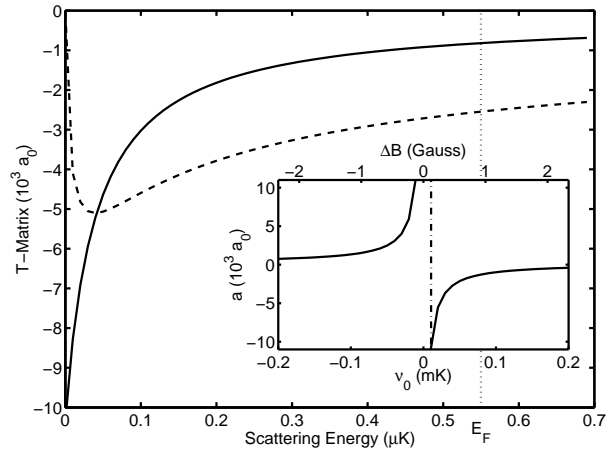


Figure 5.1: Real (solid line) and imaginary (dashed line) components of the  $T$ -matrix for collisions of the lowest two spin states of  $^{40}\text{K}$  at a detuning of  $20 E_F$ , shown in length dimensions, i.e.,  $T_k/(4\pi\hbar^2/m)$ . The inset shows the scattering length as a function of detuning, with  $20 E_F$  detuning indicated by the dashed-dot line.

### 5.1 Signatures

In this chapter we will develop a Feshbach resonance field theory for interacting Fermi gases and show that the enhanced interactions do indeed increase the critical temperature. Once the critical point is reached it remains to distinguish a clear signature of the phase transition. Various approaches have been proposed to detect the superfluid state: measurements of the pair distribution [60, 61], experiments involving the breakup

of Cooper pairs [62], measurements of the moment of inertia [63], and probes of collective excitations [64, 65, 66]. In this chapter we will show that a more direct signature of the transition to superfluidity is provided by the density distribution in an inhomogeneous system. We demonstrate that, in a harmonic trap, the superfluid state manifests in the appearance of a density bulge in the central atomic density.

## 5.2 Resonant Hamiltonian for a Fermi gas

We will now extend the concepts of BCS theory, detailed in the last chapter, and well accounted for in the literature of trapped atomic gases [67, 68, 69, 70, 71], to incorporate resonantly interacting Fermi gases [49, 72]. To begin, we consider a resonance such as that of  $^{40}\text{K}$ , illustrated in Fig. 5.1, for  $s$ -wave scattering of atoms in the lowest two hyperfine spin states  $\sigma \in \{\uparrow, \downarrow\}$ . The scattering length is the intercept at zero scattering energy which, for this case, is approximately  $-10000 a_0$ , where  $a_0$  is the Bohr radius. The large variation in the  $T$ -matrix over the relevant energy range indicates that a quantum field theory developed from this microscopic basis will need to correctly incorporate this strong energy dependence. The inset shows the resonant form of the scattering length which obeys the usual dispersive form  $a = a_{\text{bg}}(1 - \kappa/\bar{\nu})$ . For  $^{40}\text{K}$ , the dispersion parameters are  $a_{\text{bg}} = 176 a_0$  and  $\kappa = 0.657 \text{ mK}$ [73].

In analogy to the Hamiltonian presented in Eq. (3.2), we write down the following Hamiltonian for the Fermi system:

$$\begin{aligned}
H &= \sum_{\sigma} \int d^3x \psi_{\sigma}^{\dagger}(\mathbf{x}) H_{\sigma}(x) \psi_{\sigma}(\mathbf{x}) + \int d^3x \psi_m^{\dagger}(\mathbf{x}) H_m(x) \psi_m(\mathbf{x}) \\
&+ \int d^3x d^3x' \psi_{\downarrow}^{\dagger}(\mathbf{x}) \psi_{\uparrow}^{\dagger}(\mathbf{x}') U(\mathbf{x} - \mathbf{x}') \psi_{\uparrow}(\mathbf{x}) \psi_{\downarrow}(\mathbf{x}) \\
&+ \int d^3x d^3x' \left( \psi_m^{\dagger}\left(\frac{\mathbf{x} + \mathbf{x}'}{2}\right) g(\mathbf{x} - \mathbf{x}') \psi_{\downarrow}(\mathbf{x}) \psi_{\uparrow}(\mathbf{x}') + \text{h.c.} \right). \quad (5.1)
\end{aligned}$$

We define the free atomic dispersion for each spin state as  $H_{\sigma}(x) = -\frac{\hbar^2}{2m} \nabla_x^2 + V_{\sigma}(\mathbf{x}) - \mu_{\sigma}$  and the free molecular dispersion as  $H_m(x) = -\frac{\hbar^2}{4m} \nabla_x^2 + V_m(\mathbf{x}) - \mu_m$ .  $V_{\sigma,m}$  are the external potentials and  $\mu_{\sigma,m}$  are the various chemical potentials for each species. The

Feshbach resonance is controlled by the magnetic field which is incorporated by the detuning  $\nu = \mu_m - \mu_\uparrow - \mu_\downarrow$  between the chemical potential of each of the two spin states and the molecular fields.

The field operators  $\psi_\sigma^\dagger(\mathbf{x}), \psi_\sigma(\mathbf{x})$  create and destroy atoms of spin  $\sigma$  at point  $\mathbf{x}$  and  $\psi_m^\dagger(\mathbf{x}), \psi_m(\mathbf{x})$  create and destroy molecules at point  $\mathbf{x}$ . The atomic field operators now commute like fermions whereas the molecular fields retain a bosonic nature:

$$\begin{aligned} \left[ \psi_{\sigma_1}(\mathbf{x}), \psi_{\sigma_2}^\dagger(\mathbf{x}') \right]_A &= \delta_{\sigma_1, \sigma_2} \delta^3(\mathbf{x} - \mathbf{x}'), \\ \left[ \psi_m(\mathbf{x}), \psi_m^\dagger(\mathbf{x}') \right] &= \delta^3(\mathbf{x} - \mathbf{x}'), \end{aligned} \quad (5.2)$$

where the above subscript  $A$  refers to anti-commutation. The bosonic nature of the molecular field, although comprised of a pair of fermions, is justified with the understanding that the closed channel molecules are extremely well bound and have a relative size much smaller than all other length scales in the problem. They, therefore, are well characterized as bosons.

We now consider the general structure of the theory for the homogeneous case. Equation (5.1) is written in position space, however, we would now like to change to momentum space. This may be done by introducing the plane wave expansion of the operators:

$$\begin{aligned} \psi_\sigma(\mathbf{x}) &= \frac{1}{\sqrt{V}} \sum_{\mathbf{k}} a_{\mathbf{k}\sigma} e^{i\mathbf{k}\cdot\mathbf{x}} \\ \psi_m(\mathbf{x}) &= \frac{1}{\sqrt{V}} \sum_{\mathbf{k}} b_{\mathbf{k}} e^{i\mathbf{k}\cdot\mathbf{x}}, \end{aligned} \quad (5.3)$$

in a volume  $V$ . With this expansion, Eq. (5.1) transforms to:

$$\begin{aligned} H &= \sum_{\mathbf{k}\sigma} (\epsilon_{\mathbf{k}\sigma} - \mu_\sigma) a_{\mathbf{k}\sigma}^\dagger a_{\mathbf{k}\sigma} + \sum_{\mathbf{k}} (\epsilon_{\mathbf{k}m} + \nu) b_{\mathbf{k}}^\dagger b_{\mathbf{k}} \\ &+ U \sum_{\mathbf{q}\mathbf{k}\mathbf{k}'} a_{\mathbf{q}/2+\mathbf{k}\uparrow}^\dagger a_{\mathbf{q}/2-\mathbf{k}\downarrow}^\dagger a_{\mathbf{q}/2-\mathbf{k}'\downarrow} a_{\mathbf{q}/2+\mathbf{k}'\uparrow} + g \sum_{\mathbf{k}\mathbf{q}} \left( b_{\mathbf{q}}^\dagger a_{\mathbf{q}/2-\mathbf{k}\downarrow} a_{\mathbf{q}/2+\mathbf{k}\uparrow} + \text{h.c.} \right), \end{aligned} \quad (5.4)$$

where h.c. denotes the hermitian conjugate. The free dispersion relation for the fermions and bosons respectively are  $\epsilon_{\mathbf{k}\sigma} = \hbar^2 k^2 / 2m$  and  $\epsilon_{\mathbf{k}m} = \hbar^2 k^2 / 4m$ , and  $\nu$  denotes the

detuning of the boson resonance state from the zero edge of the collision continuum. In deriving Eq. (5.4) we have introduced contact potentials so must again renormalize as in Appendix A.1.

### 5.3 Construction of dynamical equations for fermions

From this Hamiltonian (Eq. (5.4)), we construct the dynamical Hartree-Fock-Bogoliubov (HFB) equations for both the bosonic and fermionic mean-fields. These equations involve the mean fields corresponding to the spin density  $n = \sum_{\mathbf{k}} \langle a_{\mathbf{k}\sigma}^\dagger a_{\mathbf{k}\sigma} \rangle$  (taken to be identical for both spins), the pairing field  $p = \sum_{\mathbf{k}} \langle a_{-\mathbf{k}\downarrow} a_{\mathbf{k}\uparrow} \rangle$ , and the condensed boson field  $\phi_m = \langle b_{\mathbf{k}=0} \rangle$ . Note that since we only consider the condensate portion of molecules, and are dealing with a homogeneous system, we may neglect the kinetic contribution of the molecules. The single particle density matrix [54] is defined as:

$$\mathcal{G}_{i,j} = \langle A_j^\dagger A_i \rangle, \quad A = \begin{pmatrix} a_{\mathbf{k}\uparrow} \\ a_{\mathbf{k}\downarrow} \\ a_{-\mathbf{k}\uparrow}^\dagger \\ a_{-\mathbf{k}\downarrow}^\dagger \end{pmatrix}, \quad (5.5)$$

and evolves according to the Bogoliubov self-energy  $\Sigma$

$$i\hbar \frac{d\mathcal{G}}{dt} = [\Sigma, \mathcal{G}]. \quad (5.6)$$

The differences between Eq. (5.6) and Eq. (3.10) arise due to the particle statistics. The self-energy for fermions now has a Hermitian structure

$$\Sigma = \begin{pmatrix} U_k & 0 & 0 & \Delta \\ 0 & U_k & -\Delta & 0 \\ 0 & -\Delta^* & -U_k & 0 \\ \Delta^* & 0 & 0 & -U_k \end{pmatrix}, \quad (5.7)$$

where the single particle energy is  $U_k = \epsilon_k - \mu + Un$ , we define a gap  $\Delta = Up + g\phi_m$ , and  $\mu$  is the chemical potential. Finally, the dynamical equations are closed by the

evolution equation for the boson mode:

$$i\hbar \frac{d\phi_m}{dt} = \nu \phi_m + g p. \quad (5.8)$$

#### 5.4 Application to a trapped system

In order to solve this set of equations, the self-energy  $\Sigma$  is diagonalized locally at each  $k$  by the Bogoliubov transformation (see Appendix B) generating quasi-particles with an energy spectrum  $E_k = \sqrt{U_k^2 + |\Delta|^2}$ . In equilibrium, the quasi-particle states are occupied according to the Fermi-Dirac distribution  $n_k = [\exp(\beta E_k) + 1]^{-1}$ . The corresponding maximum entropy solution for the molecule amplitude is found by  $i\hbar d\phi_m/dt = \mu_m \phi_m$ , where  $\mu_m = 2\mu$ , so that Eq. (5.8) implies

$$\phi_m = g p / (\mu_m - \nu). \quad (5.9)$$

The mean fields can then be determined by integration of the equilibrium single particle density matrix elements given by:

$$\begin{aligned} n &= \frac{1}{(2\pi)^2} \int_0^K dk k^2 [(2n_k - 1) \cos 2\theta_k + 1], \\ p &= \frac{1}{(2\pi)^2} \int_0^K dk k^2 (2n_k - 1) \sin 2\theta_k, \end{aligned} \quad (5.10)$$

where  $\tan 2\theta_k = |\Delta|/U_k$  is the Bogoliubov transformation angle. Since  $\theta_k$  depends on  $n$  and  $p$ , these equations need to be solved self-consistently. As a technical point, it should be noted that the  $p = 0$  solution should be discarded when the superfluid state is present since it then corresponds to an unstable point on the free energy surface.

Perhaps it is useful to rewrite Eqs. (5.10) in the following form

$$\begin{aligned} 1 &= - \left( U - \frac{g^2}{\nu - 2\mu} \right) \int \frac{d^3k}{(2\pi)^3} \frac{\tanh(\beta E_{\mathbf{k}}/2)}{2E_{\mathbf{k}}} \\ n &= \frac{1}{2} \int \frac{d^3k}{(2\pi)^3} \left( 1 - \frac{U_{\mathbf{k}}}{E_{\mathbf{k}}} \tanh(\beta E_{\mathbf{k}}/2) \right). \end{aligned} \quad (5.11)$$

The form of Eqs. (5.11) clearly relate the resonance equations to the BCS gap and number equation (Eqs. (4.18) and (4.19)).

So far this theory has been presented for a homogeneous system, while we are interested in a gas of  $N$  atoms confined to an external trapping potential  $V(\mathbf{r})$ . However, a full quantum mechanical treatment of the trapping states is not required. For instance, in our case, with a temperature on the order of  $T = 0.2T_F$ , the harmonic oscillator level spacing is smaller than both the Fermi and thermal energies. Under these conditions, we may incorporate the effect of the trap through a semi-classical, local-density approximation [75, 76]. This involves replacing the chemical potential by a local one

$$\mu(\mathbf{r}) = \mu - V(\mathbf{r}), \quad (5.12)$$

and determining the thermodynamic solution at each point in space as for the homogeneous system.

In general, the validity of the semi-classical approximation requires a slow variation in the occupation of the discrete quantum levels as a function of energy. Remarkably, in both bosonic and fermionic gases, this condition can often be satisfied even at very low temperatures because of strong correlations in a BEC due to repulsive interactions and because of exchange effects in a quantum Fermi gas. In both cases, the zero temperature, semi-classical approximation for dilute gases is usually referred to as the Thomas-Fermi approximation.

## 5.5 Thermodynamic results and signatures of superfluidity

We evaluate the thermodynamic quantities at given  $T$  and  $N$  in three steps:

- (1) For given  $\mu$ , we determine the local chemical potential  $\mu(\mathbf{r}) = \mu - V(\mathbf{r})$  and use this value to find the self-consistent solution for the density  $n(\mathbf{r})$  and pairing field  $p(\mathbf{r})$  at each point in space, according to the solution of Eqns. (5.10).
- (2) We modify the global chemical potential  $\mu$  until the density integral  $N = \int d^3r n(\mathbf{r})$  gives the desired atom number.

- (3) We use the resulting solution for  $\mu$  to calculate observable quantities, such as the density, gap, compressibility, and so forth.

The resulting solution for the density distribution is illustrated in Fig. 5.2. A striking signature of the resonance superfluidity is evident in the predicted density profile which has a notable bulge in the region of the trap center. This signature would appear to be directly accessible experimentally. One approach to measure this density bulge would be to fit the expected density profile for a quantum degenerate gas with no superfluid phase to the wings of the distribution (outside the dotted lines shown in Fig. 5.2). The excess density observed at the trap center could then be recorded. Fig. 5.3 illustrates the emergence of the superfluid as the temperature is decreased. Qualitatively, this situation is reminiscent of the central condensate peak observed for a Bose-Einstein condensed gas in a harmonic potential.

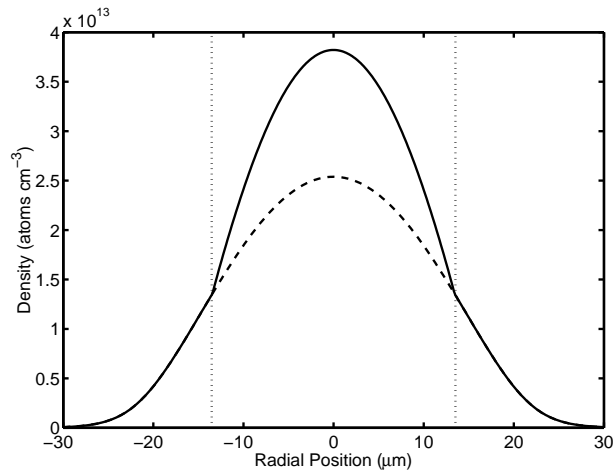


Figure 5.2: Density profile at temperature  $T = 0.2T_F$  and detuning  $\nu = 20 E_F$  showing accumulation of atoms at the trap center (solid line). We compare with the profile resulting from the same  $\mu$  but artificially setting the pairing field  $p$  to zero so that no superfluid is present (dashed line).

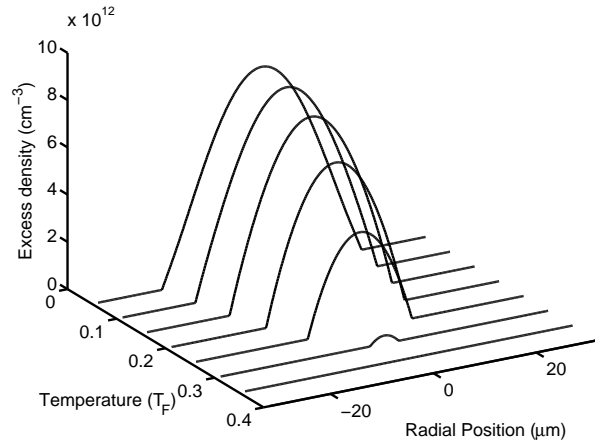


Figure 5.3: Emergence of the coherent superfluid for  $\nu = 20 E_F$ . The superfluid occupies an increasing volume as the temperature is reduced. Shown is the excess density (difference between the dashed and solid lines in Fig. 5.2) at each temperature.

We explain the observed behavior by considering the compressibility of the normal and superfluid gas. Thermodynamically, the isothermal compressibility  $C$  is defined as

$$C^{-1} = n(\partial P / \partial n)_T, \quad (5.13)$$

where  $P$  is the pressure and is shown in Fig. 5.4. The compressibility is positive everywhere, indicating that, in spite of the large attractive interactions, the Fermi pressure makes the configuration mechanically stable. A significant feature is the discontinuous behavior at the radius from the trap center at which the superfluid changes from zero to a non-zero value. This discontinuity is a manifestation of a second-order phase transition occurring in space. The discontinuity is a consequence of the local density approximation and cannot occur in a finite system. However, a rapid change in the compressibility is expected. In principle, this could be probed by studies of shock waves generated by the abrupt jump in the speed of sound as a density fluctuation passes through the discontinuous region.

## 5.6 Conclusions

This section has shown how we may derive a resonant theory for dilute Fermi gases and has applied this theory to the case of a trapped ensemble. We demonstrated that there exists a direct signature of superfluidity in trapped Fermi gases. The onset of superfluidity leads to a density bulge in the center of the trap which can be detected by absorption imaging. The critical conditions for superfluidity are satisfied initially in the trap center and the region of non-zero pairing field spreads out from the center as the temperature is lowered further. The increase in the density profile in the superfluid region is caused by a jump in the compressibility. Direct measures of this behavior are possible by the study of the propagation of sound waves. We have applied our method here to  $^{40}\text{K}$ , but a similar approach is easy to derive for other interesting atoms, including, in particular,  $^6\text{Li}$  which is another fermionic alkali currently being investigated experimentally.

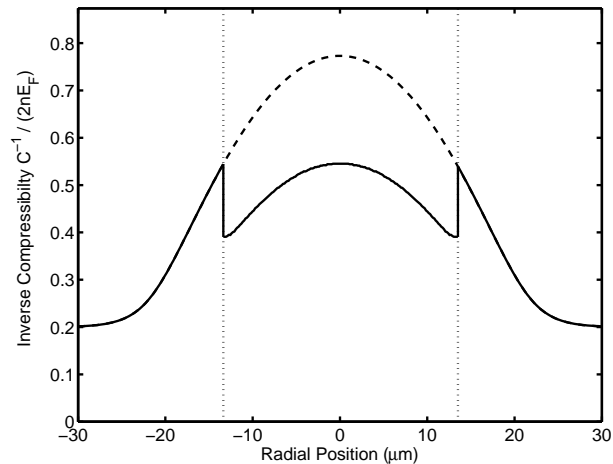


Figure 5.4: Inverse isothermal compressibility  $C^{-1}$  in units of the Fermi energy (solid line). Here  $\nu = 20 E_F$  and  $T = 0.2 T_F$  (as can be seen from the limiting behavior at large radial position). A discontinuity appears at the radius at which the superfluid emerges (dotted line). We compare this solution to that corresponding to zero pairing field and no superfluid phase transition (dashed line).